



Photocatalyst treatment for lead(II) using titanium oxide nanoparticles embedded in PVA-alginate beads

Ani Idris^{a,*}, Zohreh Majidnia^a, Khairol Sozana bt. Nor Kamarudin^b

^aFaculty of Chemical Engineering, Department of Bioprocess Engineering, c/o Institute of Bioproduct Development, Universiti Teknologi Malaysia, Skudai 81310, Johor, Malaysia, Tel. +60 07 5535603; Fax: +60 07 5581463; email: ani@cheme.utm.my (A. Idris), Tel. +60 17753 793; email: zmajidnia@yahoo.com (Z. Majidnia)

^bFaculty of Chemical Engineering, Department of Gas Engineering, Universiti Teknologi Malaysia, Skudai 81310, Johor, Malaysia, Tel. +60 75535482; email: sozana@fkkksa.utm.my

Received 17 April 2014; Accepted 16 December 2014

ABSTRACT

In this paper, titanium oxide nanoparticles were produced using the hydrothermal method and embedded in PVA–alginate beads to remove Pb(II) ions from aqueous solutions. The kinetics of the photocatalyst process was elucidated by varying operating parameters such as pH (3, 7 and 10) and initial Pb(II) concentrations (25, 50, 100 and 200 mg/L). The findings revealed that 99.1% of the Pb(II) was removed within 150 min and maximum removal occurred in initial concentration of 25 mg/L at pH 7. The titania PVA-alginate beads can be readily isolated from the aqueous solutions after the photocatalytic process and reused for at least seven times without significant loss in their initial properties. In addition, the reduction of Pb(II) from wastewater using titania PVA-alginate beads fitted the Langmuir–Hinshelwood kinetic model with a correlation coefficient (R^2) of 0.9931.

Keywords: Photocatalysts; TiO₂ nanoparticles; PVA–alginate; Pb(II) solution; Wastewater treatment

1. Introduction

The presence of heavy metals ions in industrial wastewaters is an important source of environmental pollution. Pb, Cu, Hg, Cd, Cr and Ni are the major trace elements that can be classified as the most harmful materials for public health. These toxic heavy metals are released into the environment by different ways such as, coal combustion, automobile emissions, mining activities, sewage wastewaters and the utilization of fossil fuels [1]. There are many kinds of techniques which include filtration, adsorption,

reverse osmosis, solvent extraction and membrane to separate heavy metals from aqueous solutions. Adsorption has been proved as an economically alternative method for the removal of heavy metal ions from wastewater [2].

Since Fujishima and Honda [3] discovered the photocatalytic splitting of water on TiO₂ electrodes, TiO₂ has been employed as a semiconductor photocatalyst for solar systems and environmental purification. TiO₂ photocatalysts have a synergistic effect on oxidation of organics and metal reduction, so it was applied for environment. Most of the researches were focused on the suspension of TiO₂ fine powders because they possess higher photocatalytic activity than in the form of

*Corresponding author.

thin films. But, the application of common powder catalysts has been disapproved for some reasons, due to the requirement of continuous stirring during reaction and separation difficulty after the reaction. TiO_2 can be reflected as a stable photocatalyst due to the large band gap ($E_b = 3.2$ eV); it becomes active only within the ultraviolet region that is less than 10% of the total solar intensity [4].

Some researchers [5] studied the photocatalytic properties of nanostructured TiO_2 ultrafine powder for Pb(II) removal in initial concentration of 150 mg/g under UV light. The results shown in the rate of Pb(II) removal was 100% after 1 h. In another study [6], lead(II) ions removal from aqueous solutions was performed using chitosan/ TiO_2 hybrid film and was found that the Pb(II) uptake efficiency was largely dependent on pH levels. Optimal Pb(II) adsorption conditions were within the range of pH 3–4 and initial metal concentration of 50–55 mg/L. In these conditions, the efficiency of theoretical adsorption was found to be 90.6%. Recillas et al. [6,7] applied TiO_2 nanoparticles for Pb(II) removal and the Pb^{2+} adsorption capacity was 45%. Collazo et al. [8] in his studies developed a novel synthesis method for the N-doped TiO_2 photocatalyst and the results revealed that the N-doped anatase TiO_2 was an optimal photocatalyst under visible light and sunlight irradiation, and the N-doped sample demonstrated the rate of reduction near 95%.

Alginate is one of the most widely studied natural polymers for heavy metal ions removal because it is inexpensive, non-toxic and has an efficient adsorption capacity. The carboxylate functional group of this polysaccharide is found to be responsible in capturing the heavy metal cations such as Cd(II), Pb(II) and Cu (II) [9]. However, alginate on its own is very fragile and cannot be recycled. Thus, it is usually combined with polyvinyl alcohol (PVA), the most common material used in the immobilization process because of its elasticity and high strength, and the beads produced proved to be very strong and durable [10].

Recently, the use of photocatalyst such as $\gamma\text{-Fe}_2\text{O}_3$ nanoparticles in PVA–alginate beads has been used for the reduction of metals such as Cr(VI), Pb(II) and Cd(II), respectively [11–13]. The removal of Pb(II) ions using the beads-included TiO_2 has not been explored. In most of the researches mentioned earlier, TiO_2 nanoparticles were employed either in powder or in a film form. Thus, in the current work, TiO_2 nanoparticles are embedded in PVA–alginate as matrix and they are used as a photocatalyst for the removal of Pb(II). It is hoped that these beads enable the possibility of enhancing metal retention and also create an ease for separation along with the improved bead strength.

2. Experimental

2.1. Materials

Titanium isopropoxide, acetylacetone, urea, alginate and PVA were purchased from Sigma-Aldrich. Ethanol and Pb(II) solution were purchased from Merck.

2.2. Method

2.2.1. TiO_2 powder synthesis

Initially, 2 mL of acetylacetone and 2 mL of titanium isopropoxide were mixed together and then added to 40 mL of ethanol at room temperature. The mixture and the urea solution (0.5 g of urea in 10 mL deionized water) were then added drop wise in 40 mL of deionized water with continuously stirring at room temperature. The resulting mixture was pale yellow in colour with a pH value of 5.6. The mixture was vigorously stirred for 1 h and then transferred into a 120 mL Teflon-lined stainless steel autoclave, which was heated in an oven at 150°C for 18 h. The contents were allowed to cool at room temperature. The yellowish white sample was centrifuged with ethanol and deionized water. Finally, the sample was dried at 80°C for 3 h and stored in a dark coloured dry bottle which was ready for use [14].

2.2.2. TiO_2 beads preparation

About 100 mL of precursor solution was prepared by mixing 12 g of PVA, 1 g of alginate and 0.1 g of titanium oxide in distilled water. Twelve gram of PVA was initially stirred in 72 mL of distilled water for about 5 h under conventional heating at 80°C, while alginate was stirred in 20 mL of distilled water in a different beaker. PVA was subsequently heated in a microwave for another 4 min to ensure complete dissolution. The alginate and titanium oxide powder were added to PVA solutions in a beaker. To ensure homogeneity, the solution was continuously stirred. The solution was then pumped through a peristaltic pump through a pipette into the solution containing 6 wt.% boric acid and 2 wt.% calcium chloride (CaCl_2). Then, the beads were left in the solution for 24 h and were washed with distilled water several times, and stored in deionized water for future use [11,15].

2.2.3. Characterization of the TiO_2 nanoparticles

TiO_2 nanoparticles were identified with an X-ray ($2\theta = 20\text{--}90$) diffractometer (XRD, Bruker D-8 Advance) using the Cu– $K\alpha$ radiation of wavelength $\lambda = 1.5406$ Å

[14]. The Fourier transform infrared spectroscopy (FTIR) spectrum was capable for quantitatively analyzing major functional groups in an adsorbent [16]. FTIR measurements are conducted within the range of 400–4,000 cm^{-1} [17]. Morphological and structural analysis of the samples were done by a field emission scanning electron microscope (FESEM, Hitachi S4800) and a high-resolution transmission electron microscope (HRTEM, JEOL-JSM-6360). Furthermore, complementary test was used to determine the Brunauer–Emmett–Teller (BET) surface area, pore diameter and volume of titania PVA–alginate beads using N_2 adsorption isotherms at 80°C with Quantachrome NovaWin 2 analyzer. The sphericity factor which describes the bead shape is defined by Eq. (1):

$$\text{Sphericity factor} = \frac{d_{\max} - d_{\text{per}}}{d_{\max} + d_{\text{per}}} \quad (1)$$

where d_{\max} (mm) and d_{per} (mm) is the maximum diameter and the perpendicular diameter to d_{\max} both passing through the titania PVA–alginate beads centroid.

2.2.4. Photocatalytic activity under sunlight

The experiments were conducted under sunlight irradiation. Ten grams of titanium oxide beads were placed in 200 mL of Pb(II) solution in a 500 mL beaker. Five millilitre samples were taken every 15 min for 180 min and analysed for Pb(II) content (Fig. 1). The initial concentrations of Pb(II) in the solutions were ranged from 25, 50, 100 to 200 mg/L [5–7,9,13,18]. The influence of pH on Pb(II) sorption was also investigated at various pH (3, 7 and 10). The

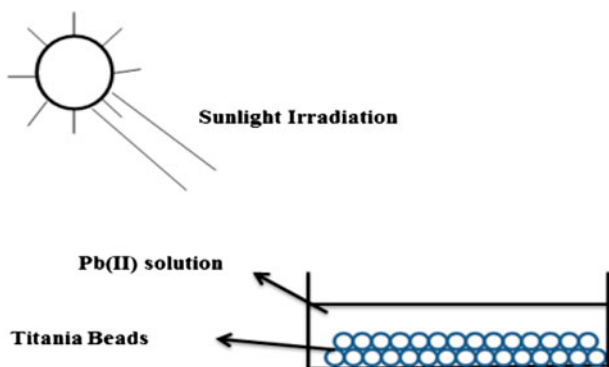


Fig. 1. Schematic diagram of photocatalytic activity under sunlight irradiation.

pH value for the initial solution was set to the required pH value through the addition of NaOH for alkaline solution or HCl for acidic solution [19]. Following the contact time, the metal ions contents were analysed.

2.2.5. Recycle ability

The titania PVA–alginate beads reusability was assessed using consecutive photocatalytic cycles. Using the same titania PVA–alginate beads, the photocatalytic experiments were repeated. The metal-loaded titania PVA–alginate beads (10 g) were washed with desorbing agent (HCl 50 mL of 0.1 M) in 250 mL Erlenmeyer flasks. In the course of every photocatalytic process, the flasks containing the beads in the HCl solution were put on a shaker and rotated at 100 rpm for 60 min at room temperature, and the supernatant was analysed for the desorbed metal ions. The atomic absorption spectrophotometer was then used to measure the concentration of Pb(II) desorbed in acidic solution. The used titania PVA–alginate beads were recycled and reused as a photocatalyst for another seven repeated cycles to study the regenerative behaviour of the photocatalyst [9,16].

3. Results and discussion

3.1. Morphology of titanium oxide nanoparticles

Fig. 2 depicts the XRD patterns of powders obtained from the hydrothermal treatment. The peaks of the powdered material were found to result from (1 0 1), (0 0 4), (2 0 0), (1 0 5), (2 1 3), (1 1 6), (2 1 5) and (3 0 3) reflections. The reflection peaks can be easily indexed to anatase TiO_2 with lattice constants of $a = 3.784 \text{ \AA}$ and $c = 9.512 \text{ \AA}$ (JCPDS: No. 84-1286). No characteristic peaks relevant to other crystalline forms were identified

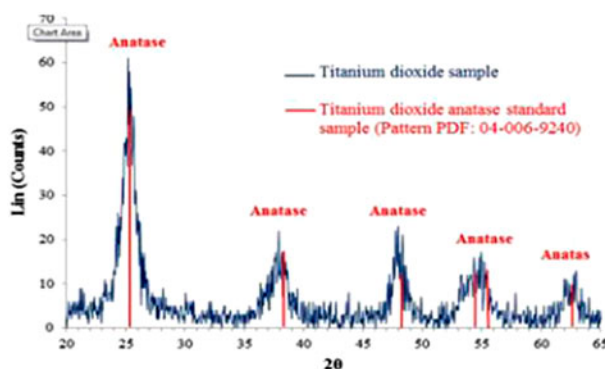


Fig. 2. XRD patterns of the as-prepared TiO_2 nanoparticles and standard TiO_2 anatase.

in the XRD pattern [10,13]. Also, as it is observed in this figure, red graph is for standard TiO_2 anatase with Pattern PDF: 04-006-9240 that with comparison of standard TiO_2 anatase nanoparticles and prepared TiO_2 anatase nanoparticles, it was found that TiO_2 nanoparticles in this study are pure [20].

The FTIR spectra of TiO_2 powder are shown in Fig. 3. The broad band between $3,200$ and $3,600\text{ cm}^{-1}$ can be observed on samples, which related to O–H stretching and deformation vibrations of weak-bound water. Also, the bands between 400 and 800 cm^{-1} were related to the vibrations of tin oxide [21], while the sharp bands in the range of $1,400$ – $1,700\text{ cm}^{-1}$ were attributed to the CH_2 - and $-\text{CH}_3$ bands.

The high- and low-magnification FESEM images of the prepared powder sample are displayed in Fig. 4((a) and (b)), respectively. The nanoparticles are uniformly distributed throughout the sample and the sizes of the particles are fairly small. The FESEM images are shown in Fig. 4((c) and (d)), which clearly shows the uniform distribution of TiO_2 nanoparticles and the average particle size obtained is found to be approximately 15 nm . The minimum and maximum particle sizes lie close to average particle size.

Fig. 5((a) and (b)) shows the cross-sectional structure and morphology of the titania PVA–alginate beads at $1,000\times$ magnification before and after photocatalysis under sunlight irradiation, respectively. The FESEM images revealed the presence of the pores, and such porous morphology contributed well to the mass

transfer of Pb(II) to the photocatalyst active sites embedded in the titania PVA–alginate beads. Upon comparing Fig. 5((a) and (b)) most of the pores were still visible, although some small pore areas (Fig. 5(b)) were seen slightly covered mainly due to the adsorption of Pb(II) ions.

Fig. 5((c) and (d)) illustrates the surface structure of titania PVA–alginate beads at $2,500\times$ magnification before and after photoreduction under sunlight irradiation, respectively. It is observed that although some of the surfaces are covered with Pb(II) ions, a majority of them are still accessible for further adsorption of Pb(II) ions. The surfaces of the titania PVA–alginate beads are observed to be porous and rough. EDX analysis was done in conjunction with the FESEM analysis to determine the elemental composition of selected spots on the titania PVA–alginate beads surface. Table 1 displays the EDX analysis of the various elements on the surface and cross-section of titania PVA–alginate beads before and after photoreduction under sunlight irradiation. It was observed that besides Ti, Ca and O, there were large amounts of residual carbon in the initial organic components. The results in Table 1 indicate that the amount of Pb(II) ions on the surface of the titania PVA–alginate beads is only 0.15% compared to the cross-section, where the iodine ions concentration was found to be very much higher at 0.83% after photoreduction. This could be attributed to the porous structure of the titania PVA–alginate beads which allows the diffusion of lead ions

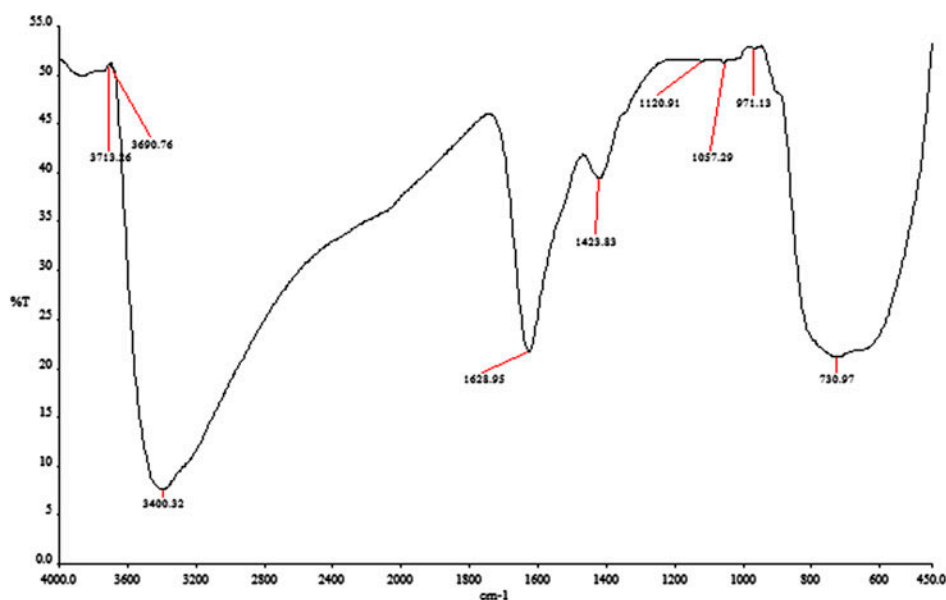


Fig. 3. FTIR analysis of titanium oxide nanoparticles.

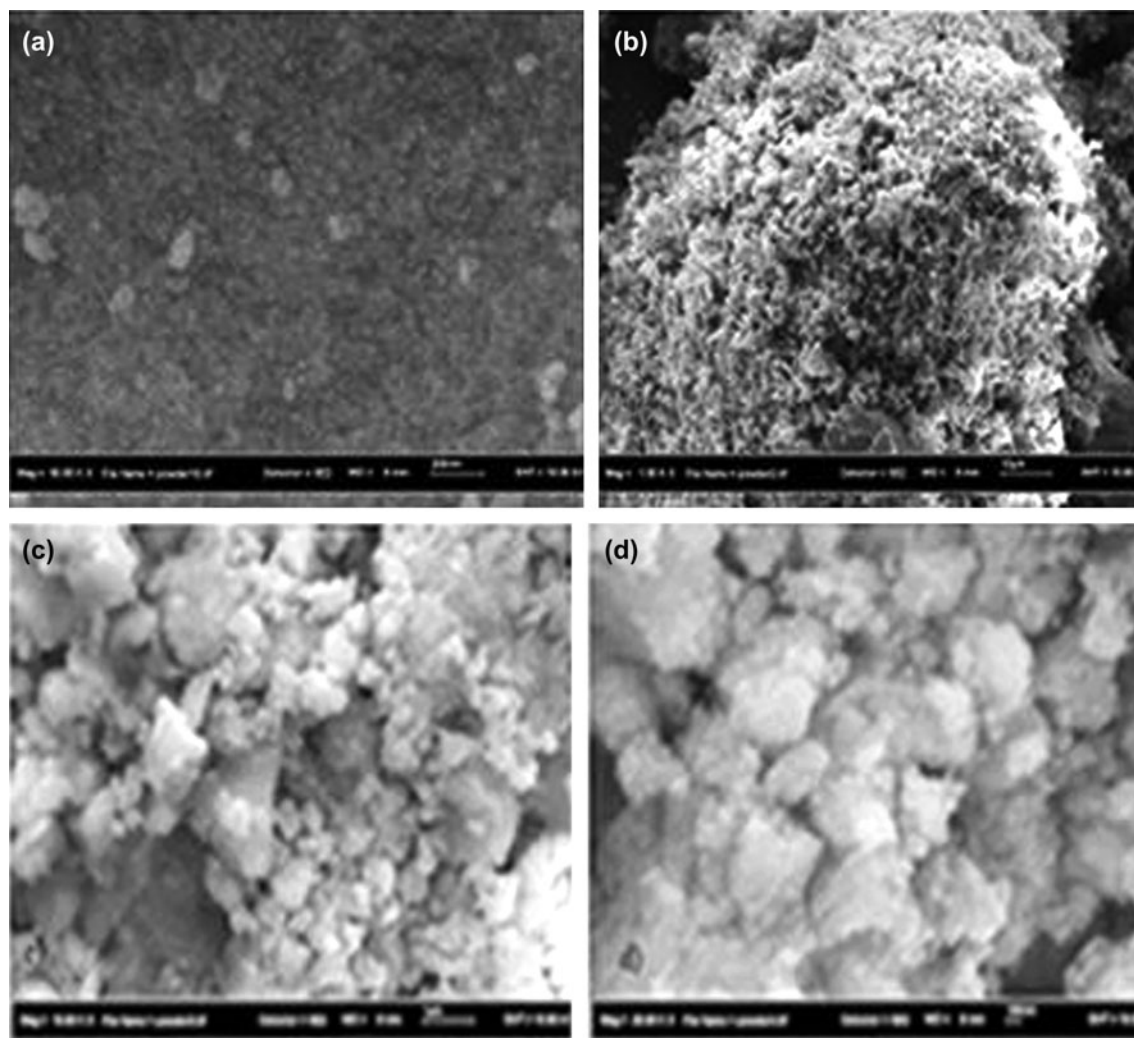


Fig. 4. (a) and (b) are the FESEM images; (c) and (d) are the FESEM images for different magnification of TiO_2 nanoparticles.

Table 1

EDX analysis of the various elements on the surface of titania PVA–alginate beads before and after process under sunlight (initial concentration = 50 mg/L)

Component	Mass percentage (%)			
	Surface of PVA–alginate		Cross section of PVA–alginate	
	Before process	After process	Before process	After process
Carbon (C)	27.50	53.21	28.24	45.12
Oxygen (O)	49.77	33.1	39.62	31.82
Sodium (Na)	0.59	0	0.53	0
Calcium (Ca)	6.4	0.89	17.41	4.92
Lead (Pb)	0.00	0.15	0	0.81
Titanium (Ti)	16.08	13.41	13.11	11.29

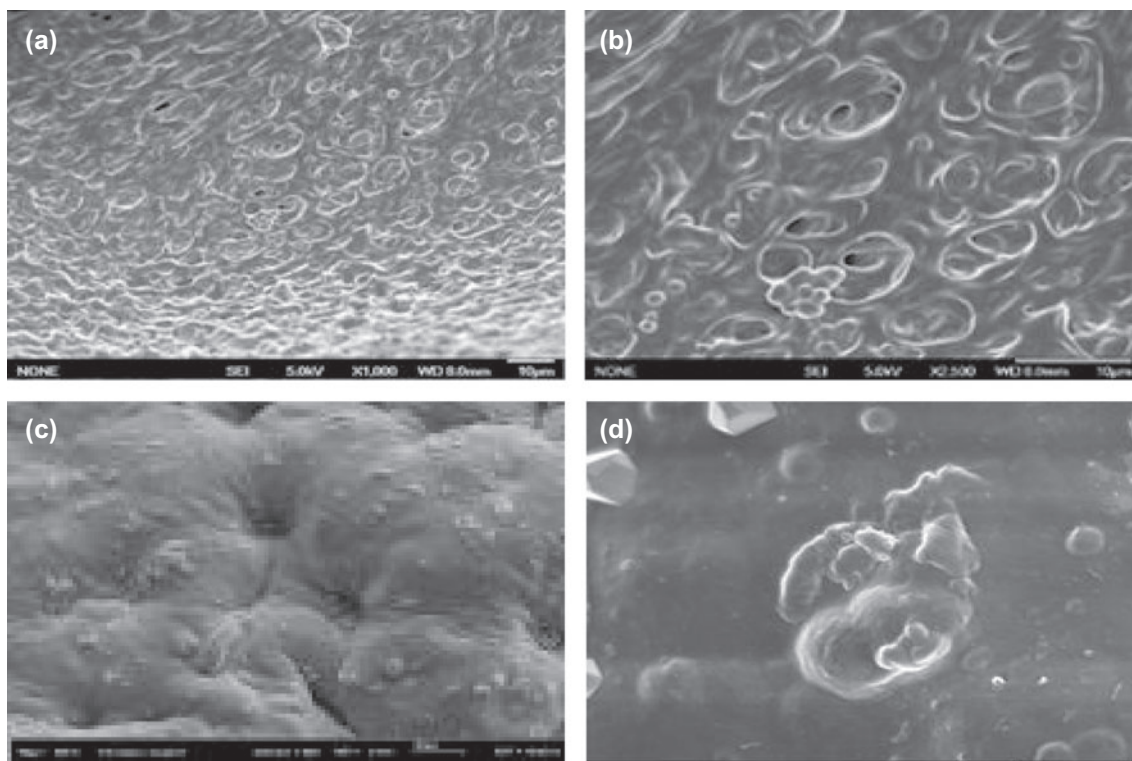


Fig. 5. FESEM images of cross section of titania PVA–alginate beads (a) before and (b) after removal of Pb(II) at 1,000× magnification; surface FESEM images of beads at 2,500× magnification (c) before and (d) after the process reaction.

into the interior of the beads, thus, resulting in higher concentrations of Pb(II) ions observed in the cross-section of the beads. This supported the hypothesis that the porous surface structure contributed well to mass transfer of the lead ions into the interior sections of the beads. The BET surface area, pore volume and pore diameter of the titania PVA–alginate beads were found to be $24.48 \text{ m}^2/\text{g}$, $9.12 \times 10^{-2} \text{ cm}^3/\text{g}$ and 2.1 nm , respectively.

3.2. Photocatalytic activity

As shown in Fig. 6, in the absence of titania PVA–alginate beads, no appreciable photoreduction occurs during the 150 min of irradiation as Pb(II) is stable and cannot be decomposed. However, in the presence of titania PVA–alginate beads, the Pb(II) photoreduction occurred after 150 min under sunlight irradiation with 99.1% reduction. The Pb(II) reduction rate was only 10% when the system was not exposed to sunlight, which shows that Pb(II) removal was due to adsorption. The results confirmed that the illumination energy is essential and is significant in the degradation of Pb(II) ions. In the system with alginate beads

without titanium oxide nanoparticles and PVA under sunlight irradiation, the rate of Pb(II) reduction is only about 11% and the rate of Pb(II) removal using PVA–alginate beads without titanium oxide beads was 14%. The percentage reduction in the Pb(II) is due to the adsorption by the alginate and PVA; also, the alginate and PVA–alginate beads were protonated and the Pb species would be bonded to the alginate and PVA–alginate beads surface.

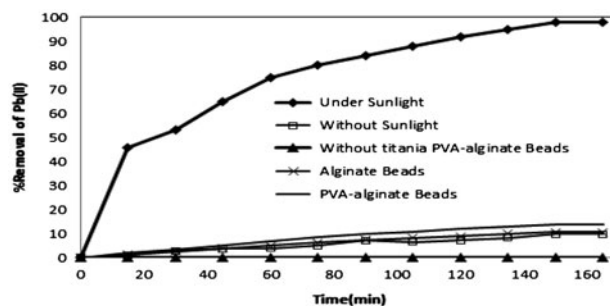


Fig. 6. Adsorption of Pb(II) on 50 mg/L concentration of Pb(II) at pH 7.

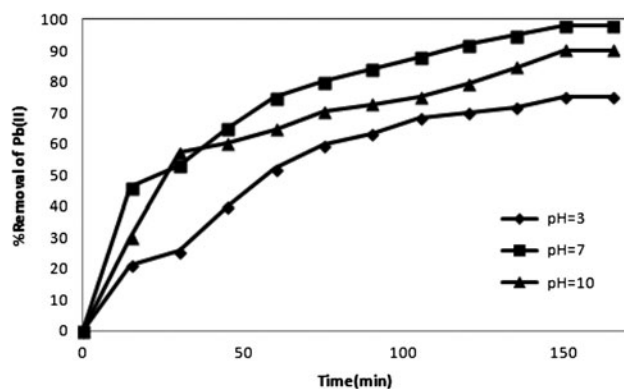


Fig. 7. Adsorption of Pb(II) ions by titania alginate beads at pH 3, 7 and 10 [experimental conditions: Pb(II) solution concentration = 50 mg/L].

3.3. Effect of pH on adsorption capacity

Fig. 7 shows Pb(II) removal at three different pH values (3, 7 and 10). Maximum Pb(II) removal occurred at pH 7. Pb(II) removal rates improved as the pH increased from 3.0 to 7.0, while a further increase in pH to 10 did not improve the Pb(II) removal.

As pH increases, the Pb(II) sorption capacity steadily increases until it reaches to pH 7 which can be explained by the fact that at lower pH more protons (H^+) are available to the carboxyl groups, thus, reducing the available binding sites in the alginate and PVA molecules.

The findings suggested that at pH 3, metal sorption was low due to the competition between Pb(II) ions and hydrogen ions (H^+) for the protonated active sites. Saeed et al. [22] made similar observations, where the heavy metal cations competed with high level of hydrogen ions available in acidic media to occupy the negative binding sites which was not a favourable condition for metal binding [23]. In alkaline media, the number of OH^- would dominate in the solution leading to less competition with the Pb(II) cations to bind at the active sites [24]. In addition to the competition binding of Pb(II) ions and hydrogen ions, the metal ions adsorption occurred through an ion-exchange mechanism by replacement of calcium for chelating of functional groups in titania PVA–alginate beads [23]. In the ionic exchange process, one calcium ion is replaced by one Pb(II) ion. Chen and Li [25] have shown that the affinity of alginate to Pb(II) is much higher than that of Ca(II) causing the ion-exchange process to occur, which Ca(II) ions petite molecule was released with simultaneous binding to the Pb(II) ions.

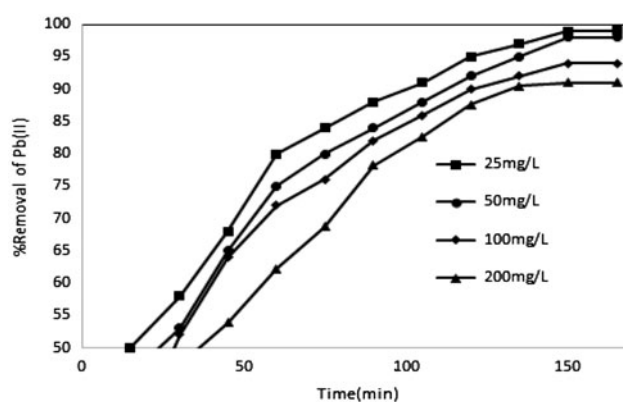


Fig. 8. Adsorption of Pb(II) ions by titania alginate beads at different initial concentrations of Pb(II) at pH 7.

3.4. Effect of initial concentration solution on adsorption capacity

Fig. 8 depicts the percentage reduction of Pb(II) as a function of illumination time at pH 7 at different initial concentrations of Pb(II). The Pb(II) ions uptake with respect to contact time occurred in two stages under all pH conditions. In the first hour of sorbent–sorbent contact, a rapid metal uptake occurred which is known as the first stage [9]. This was followed by a slower metal uptake rate and an equilibrium spreading over a considerably lower period of time known as the second stage. Such an adsorption pattern has been documented in several literature reviews for research on other metal ions or adsorbents. The rapid phase may be due to the abundant availability of active sites on the biosorbent initially. Upon gradual occupancy of these sites, sorption occurs less efficiently as demonstrated by the slower phase.

3.5. Desorption and regeneration

The desorption and regeneration potential of PVA–alginate titania beads is considered to be very important because it determines the cost associated with the adsorption system. In the present study, the Pb(II) desorption from the metal-loaded titania PVA–alginate beads occurred at pH 7 and at initial concentration of 50 mg/L. Pb(II) desorption from the metal-loaded on titania PVA–alginate beads for the first cycle led to 85.60% metal recovery. Fig. 9 shows that the percentages of desorption for the metals do not decrease remarkably during the five sorption–desorption cycles. During the first cycle, the metal-removing efficiency of Pb(II) on titania PVA–alginate beads was 85.6% while in the second cycle, it was observed as 3.7% decrease in desorption capacity of titania PVA–alginate beads.

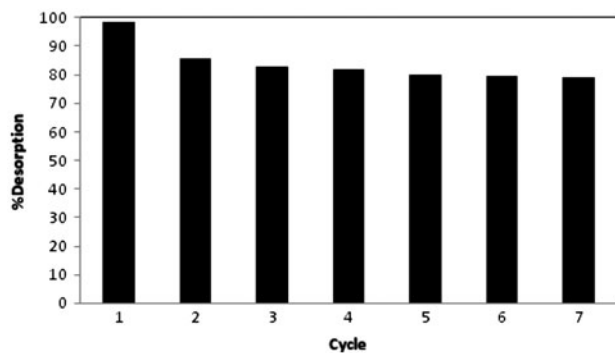


Fig. 9. Desorption capacities on recycling titanium oxide beads [experimental conditions: Pb(II) solution concentration = 50 mg/L and pH 7].

After the second cycle, only a small decrease in the sorption capacity of titania PVA–alginate beads was observed to the seventh cycle. Therefore, titania PVA–alginate beads can be recycled a minimum of 7–8 times without significantly losing their photocatalyst activities.

3.6. Kinetic modelling

Many researchers [25–27] suggest that the reduction rates of photocatalytic reduction and degradation of various inorganics over illuminated catalyst-based metal oxide fitted the Langmuir–Hinshelwood (L–H) kinetics model. The L–H kinetics relates the rate of surface catalysed reactions to the surface covered by the substrate. According to the L–H model, the unimolecular surface reaction rate is proportional to the surface coverage. The titanium oxide surfaces are covered with hydroxyl groups whose forms vary at different pH. The surface charge is neutral at pH_{zpc} . Below the pH_{zpc} , the adsorbent surface is positively charged and anion adsorption takes place. Since the surface of TiO_2 particles in aqueous solutions is covered with hydroxyl groups and water molecules, both Pb(II) and the water molecule (H_2O) can, in principle, be adsorbed on this surface via hydrogen bonds. Considering the competition for the same active sites, the L–H model can be expressed by the following equation [26]:

$$r = -\frac{dC}{dt} = k_r\theta = \frac{k_r K_{\text{LH}} C}{1 + K_{\text{LH}} C + K_{\text{H}_2\text{O}} C_{\text{H}_2\text{O}}} \quad (2)$$

where r is the photoreduction rate of the reactant (mg/L min), C is the concentration of the reactant (mg/L), t is the illumination time, k_r is the reaction rate constant (mg/L min), K_{LH} is the adsorption coefficient of the reactant (L/mg), $K_{\text{H}_2\text{O}}$ the solvent adsorption constant and $C_{\text{H}_2\text{O}}$ the concentration of the water (Eq. (2)). As $C_{\text{H}_2\text{O}} \gg C$ and $C_{\text{H}_2\text{O}}$ remains practically constant for all concentrations, the part of the catalyst covered by water is fixed. In this section, all experimental conditions, i.e. pH and catalyst dosage remained constant. Thus, C is the only variable in the initial reactions which can be expressed as follows [26]:

$$r = -\frac{dC}{dt} = \frac{k_r K_{\text{LH}} C}{1 + K_{\text{LH}} C} \quad (3)$$

During photocatalytic reduction, due to the formation of intermediates, interference in the determination of kinetics may occur because of competitive adsorption and reduction. As a result, calculations were performed at the beginning of the illuminated conversion. During this period, any changes for example, the effect of intermediates or pH changes can be discounted and the photocatalytic reduction rate can be expressed as a function of concentration:

$$r_0 = -\frac{dC}{dt} = k_r \left(\frac{k_r K_{\text{LH}} C_0}{1 + K_{\text{LH}} C_0} \right) \quad (4)$$

where r_0 is the initial photocatalytic reduction rate (mg/L min) of Pb(II) and C_0 is the initial concentration of Pb(II) (mg/L) and K_{LH} is the adsorption equilibrium constant (L/mg). For very low values of chemical concentration C_i (C_0 small) the equation takes the form of a first-order equation [27]:

$$\ln\left(\frac{C_0}{C_t}\right) = k_r K_i = k_{\text{app}} t \quad (5)$$

Table 2
Pseudo-first-order apparent constant values for Pb(II) reduction

Initial Pb(II) concentration, C_0 (mg/L)	Reaction rate, k_{app} (min^{-1})	R^2	Initial reaction rate, r_0 (mg/L min^{-1})
50	0.018	0.98	0.9
100	0.0167	0.99	1.67
200	0.0172	0.9931	3.44

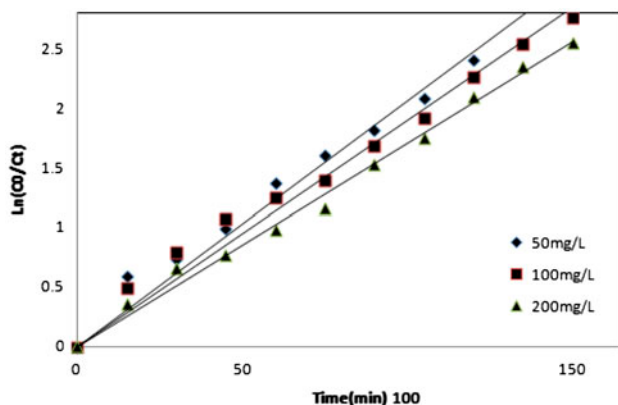


Fig. 10. Linear transform $\text{Ln } C_0/C_t = f(t)$ of the reduction of Pb(II).

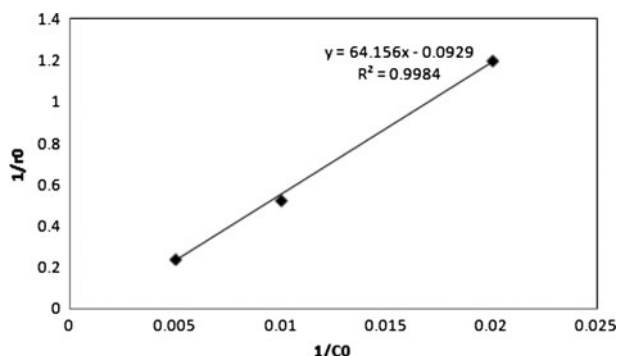


Fig. 11. The relationship between $1/r_0$ and $1/C_0$ at different initial concentrations of Pb(II).

where $k_r \cdot K = k_{\text{app}}$, C_t is the concentration of the Pb(II) at time t and C_0 is the initial concentration of the Pb(II). In general, the initial reduction rate can be obtained using the following expression:

$$r_0 = k_{\text{app}} C_0 \quad (6)$$

A straight line is obtained when $\text{Ln } (C_0/C_t)$ is plotted against time (Fig. 10). The apparent pseudo-first-order rate constant k_{app} represents the slope. Table 1 outlines the values obtained for various initial concentrations.

The following relationship holds when Eq. (3) is linearized:

$$\frac{1}{r_0} = \left(\frac{1}{k_r k_{\text{LH}}} \right) \left(\frac{1}{C_0} \right) + \left(\frac{1}{k_r} \right) \quad (7)$$

The data obtained are tabulated in Table 2 and the values of $1/r_0$ were plotted against $1/C_0$. As shown in Fig. 11, $1/r_0$ is highly correlated with $1/C_0$. Therefore, the reduction of Pb(II) by magnetic beads fitted the L–H kinetics model. In accordance with the L–H kinetics model Eq. (7), a straight line with an intercept of $1/k_r$ and a slope of $1/k_r K_{\text{LH}}$ is obtained, where k_r and K_{LH} are determined and the values are calculated to be 10.764 (mg/L min) and 0.0014 (L/mg), respectively.

The correlation coefficient (R^2) for the regression line is 0.9931. From the results obtained, it was clear that $k_r > K_{\text{LH}}$, which showed that a surface reaction, where the Pb(II) was absorbed was the controlling step in the process. These findings are in line with the results of other researchers on TiO_2 photocatalyst [26,28].

4. Conclusion

TiO_2 nanoparticles were successfully immobilized in PVA–alginate and the titania PVA–alginate beads produced can remove 99.1% of Pb(II) in less than 3 h. The titania PVA–alginate beads are superior in terms of performance, robustness and regenerative properties. They can be reused and recycled easily at least seven times without losing their initial properties throughout the process. Under sunlight irradiation, Pb(II) was almost entirely reduced within 150 min. The results show that photoreduction equilibrium can be achieved in less than 3 h within pH range of 6–10 and maximum removal occurs at neutral pH 7. The L–H kinetics model appeared to describe the photoreduction of Pb(II) on titania PVA–alginate beads rather well with k_r and K_{LH} values of 10.764 (mg/L min) and 0.0014 (L/mg), respectively, indicating that the dominating step of the process was the surface reaction where the Pb(II) was absorbed.

Symbols

E_b	—	band gap energy
DI	—	deionized water
λ	—	radiation of wavelength
r	—	photoreduction rate of the reactant (mg/L min)
C	—	concentration of the reactant (mg/L)
t	—	illumination time
k_r	—	reaction rate constant (mg/L min)
K_{LH}	—	adsorption coefficient of the reactant (L/mg)
$K_{\text{H}_2\text{O}}$	—	solvent adsorption constant
$C_{\text{H}_2\text{O}}$	—	concentration of the water
C_0	—	initial concentration of lead(II) (mg/L)
k_{app}	—	pseudo-first-order rate constant
R^2	—	correlation coefficient

References

- [1] S. Karabulut, A. Karabakan, A. Denizli, Y. Yürüm, Batch removal of copper(II) and zinc(II) from aqueous solutions with low-rank Turkish coals, *Sep. Purif. Technol.* 18 (2000) 177–184.
- [2] S. Doyurum, A. Çelik, Pb(II) and Cd(II) removal from aqueous solutions by olive cake, *J. Hazard. Mater.* 138 (2006) 22–28.
- [3] A. Fujishima, K. Honda, Photolysis-decomposition of water at the surface of an irradiated semiconductor, *Nature* 238 (1972) 38–45.
- [4] J. Yu, J.C. Yu, B.C.A.X. Zhao, Photocatalytic activity and characterization of the sol-gel derived Pb-doped TiO₂ thin films, *J. Sol-Gel Sci. Technol.* 24 (2002) 39–48.
- [5] S.J. Kim, E.G. Lee, S.D. Park, C.J. Jeon, Y.H. Cho, C.K. Rhee, W.W. Kim, Photocatalytic effects of rutile phase TiO₂ ultrafine powder with high specific surface area obtained by a homogeneous precipitation process at low temperatures, *J. Sol-Gel Sci. Technol.* 22 (2001) 63–74.
- [6] Y. Tao, L. Ye, J. Pan, Y. Wang, B. Tang, Removal of Pb (II) from aqueous solution on chitosan/TiO₂ hybrid film, *J. Hazard. Mater.* 161 (2009) 718–722.
- [7] S. Recillas, A. García, E. González, E. Casals, V. Puentes, A. Sánchez, X. Font, Use of CeO₂, TiO₂ and Fe₃O₄ nanoparticles for the removal of lead from water Toxicity of nanoparticles and derived compounds, *Desalination* 277 (2011) 213–220.
- [8] G.C. Collazzo, E.L. Foletto, S.L. Jahn, M.A. Villetti, Degradation of direct black 38 dye under visible light and sunlight irradiation by N-doped anatase TiO₂ as photocatalyst, *J. Environ. Manage.* 98 (2012) 107–111.
- [9] A. Idris, N.S.M. Ismail, N. Hassan, E. Misran, A.F. Ngomsik, Synthesis of magnetic alginate beads based on maghemite nanoparticles for Pb(II) removal in aqueous solution, *J. Ind. Eng. Chem.* 18 (2012) 1582–1589.
- [10] Z. Majidnia, A. Idris, Evaluation of cesium removal from radioactive waste water using maghemite PVA-alginate beads, *Chem. Eng. J.* 262 (2015) 372–382.
- [11] A. Idris, E. Misran, N.M. Yusof, Photocatalytic reduction of Cr(VI) by PVA-alginate encapsulated γ -Fe₂O₃ magnetic beads using different types of illumination lamp and light, *J. Ind. Eng. Chem.* 18 (2012) 2151–2156.
- [12] M.A.A. Rahman, E. Misran, A. Idris, N.M. Yusof, Removal of cadmium using ferro magnetic gels, *J. Technol.* 67 (2014) 5–9.
- [13] A. Idris, Z. Majidnia, Photo catalytic reduction of Pb (II) using titanium oxide PVA-alginate beads under sunlight, *Appl. Mech. Mater.* 606 (2014) 99–103.
- [14] R. Thapa, S. Maiti, T.H. Rana, U.N. Maiti, Anatase TiO₂ nanoparticles synthesis via simple hydrothermal route: Degradation of Orange II, methyl orange and Rhodamine B, *J. Mol. Catal. A: Chem.* 363–364 (2012) 223–229.
- [15] A. Idris, Z. Majidnia, Evaluation of the Cd removal efficacy from aqueous solutions using titania PVA-alginate beads, *Desalin. Water Treat.* (2014) 1–8.
- [16] M. Iqbal, A. Saeed, S.I. Zafar, FTIR spectrophotometry, kinetics and adsorption isotherms modeling, ion exchange, and EDX analysis for understanding the mechanism of Cd²⁺ and Pb²⁺ removal by mango peel waste, *J. Hazard. Mater.* 164 (2009) 161–171.
- [17] A.K. Yewale, F.C. Raghuvanshi, N.G. Belsare, R.V. Waghmare, R.V. Joat, T.S. Wasnik, K.B. Raulkar, A.S. Wadkatkar, G.T. Lamdhade, Gas sensitivity of TiO₂ based thick film sensor to NH₃ gas at room temperature, *Int. J. Adv. Eng. Technol.* 2 (2011) 226–230.
- [18] K. Kabra, R. Chaudhary, R.L. Sawhney, Solar photocatalytic removal of Cu(II), Ni(II), Zn(II) and Pb(II): Speciation modeling of metal-citric acid complexes, *J. Hazard. Mater.* 155 (2008) 424–432.
- [19] A. Idris, N. Hassan, R. Rashid, A.F. Ngomsik, Kinetic and regeneration studies of photocatalytic magnetic separable beads for chromium (VI) reduction under sunlight, *J. Hazard. Mater.* 186 (2011) 629–635.
- [20] A. Esfandiyari Bayat, R. Junin, A. Samsuri, A. Piroozian, M. Hokmabadi, Impact of metal oxide nanoparticles on enhanced oil recovery from limestone media at several temperatures, *Energy Fuels* 28 (2014) 6255–6266.
- [21] F. Sala, F. Trifirò, Oxidation catalysts based on tin-antimony oxides, *J. Catal.* 34 (1974) 68–78.
- [22] A. Saeed, M. Waheed Akhter, M. Iqbal, Removal and recovery of heavy metals from aqueous solution using papaya wood as a new biosorbent, *Sep. Purif. Technol.* 45 (2005) 25–31.
- [23] A.F. Ngomsik, A. Bee, J.M. Siaugue, V. Cabuil, G. Cote, Nickel adsorption by magnetic alginate microcapsules containing an extractant, *Water Res.* 40 (2006) 1848–1856.
- [24] R. Apiratikul, T.F. Marhaba, S. Wattanachira, P. Pavasant, Biosorption of binary mixtures of heavy metals by green macro alga, *Caulerpa lentillifera*, *J. Sci. Technol.* 26 (2004) 199–207.
- [25] Y.H. Chen, F.A. Li, Kinetic study on removal of copper(II) using goethite and hematite nano-photocatalysts, *J. Colloid Interface Sci.* 347 (2010) 277–281.
- [26] N. Guettaï, H.A. Amar, Photocatalytic oxidation of methyl orange in presence of titanium dioxide in aqueous suspension. Part I: Parametric study, *Desalination* 185 (2005) 427–437.
- [27] D. Chen, A.K. Ray, Photocatalytic kinetics of phenol and its derivatives over UV irradiated TiO₂, *Appl. Catal., B* 23 (1999) 143–157.
- [28] J. Sun, X. Wang, J. Sun, R. Sun, S. Sun, L. Qiao, Photocatalytic degradation and kinetics of Orange G using nano-sized Sn(IV)/TiO₂/AC photocatalyst, *J. Mol. Catal. A: Chem.* 200 (2006) 241–246.